Journal of Micromechanics and Microengineering

PAPER • OPEN ACCESS

Fabrication of microstructures in the bulk and on the surface of sapphire by anisotropic selective wet etching of laser-affected volumes

To cite this article: L Capuano *et al* 2022 *J. Micromech. Microeng.* **32** 125003

View the article online for updates and enhancements.

You may also like

- Amorphization of pure hafnium nanocontacts and continuous conductance control via phase transition treatment using nanosecond pulse voltage energization
Masayuki Nakanishi and Tokushi Kizuka
- Evidence for direct impact damage in metamict titanite $CaTiSiO_5$
Ekhard K H Salje, R Dean Taylor, Douglas J Safarik et al.
- Effect of carbon situating at end-of-range defects on silicon self-diffusion investigated using pre-amorphized isotope multilayers
Taiga Isoda, Masashi Uematsu and Kohei M. Itoh

This content was downloaded from IP address 202.8.112.141 on 08/06/2023 at 07:36

OPEN ACCESS
IOP Publishing
Journal of Micromechanics and Microengineering
J. Micromech. Microeng. 32 (2022) 125003 (13pp) https://doi.org/10.1088/1361-6439/ac9911

Fabrication of microstructures in the bulk and on the surface of sapphire by anisotropic selective wet etching of laser-affected volumes

L Capuano[1], J W Berenschot[2], R M Tiggelaar[3,*], M Feinaeugle[1], N R Tas[2], J G E Gardeniers[2] and G R B E Römer[1]

[1] Laser Processing, Department of Mechanics of Solids, Surfaces and Systems (MS3), Faculty of Engineering Technology, University of Twente, PO Box 217, 7500 AE Enschede, The Netherlands
[2] Mesoscale Chemical Systems, MESA+ Institute, Faculty of Science and Technology, University of Twente, PO Box 217, 7500 AE Enschede, The Netherlands
[3] MESA+ NanoLab cleanroom, MESA+ Institute, University of Twente, PO Box 217, 7500 AE Enschede, The Netherlands

E-mail: r.m.tiggelaar@utwente.nl

Received 24 June 2022, revised 26 September 2022
Accepted for publication 11 October 2022
Published 25 October 2022

Abstract

In this paper a processing technique for sapphire is presented which combines laser-induced amorphization and subsequent selective wet etching of amorphized sapphire as well as anisotropic wet etching of single-crystalline sapphire (α-Al_2O_3). Using this technique, microstructures can be realized on the surface and in the bulk of sapphire substrates. By focusing ultra-short laser pulses inside sapphire, its structure can be transformed from crystalline into amorphous. The modified material can be selectively removed using etchants, such as hydrofluoric acid or potassium hydroxide (KOH), solely dissolving the amorphized part. In this work, however, an etchant consisting of a standard solution of sulphuric acid and phosphoric acid (96 vol% H_2SO_4: 85 vol% H_3PO_4, 3:1 vol%) at 180 °C is utilized. This method allows the realization of structures which are impossible to achieve when using conventional etchants which solely dissolve the amorphized sapphire. Ultrashort pulsed laser irradiation (230 fs) is used in this study as starting point for the subsequent anisotropic etching to form microstructures on the surface or in the bulk of sapphire that are terminated by characteristic crystal planes. In particular, the appearance of etching-induced patterns formed by stacks of rhombohedra is shown for structures below the surface, whereas triangular pits are achieved in surface processing.

Keywords: sapphire, transparent materials, femtosecond laser, selective etching, anisotropic etching

(Some figures may appear in colour only in the online journal)

* Author to whom any correspondence should be addressed.

Original content from this work may be used under the terms of the Creative Commons Attribution 4.0 licence. Any further distribution of this work must maintain attribution to the author(s) and the title of the work, journal citation and DOI.

1. Introduction

Crystalline sapphire (α-Al_2O_3) is a material used in many branches of science and technology. It is transparent for wavelengths in a range spanning from ultraviolet (UV) to near-infrared, it has a hardness of 9 on the Mohs scale, it is a good electrical and thermal insulator, it has a high melting temperature of 2030 °C and is chemically inert [1]. These properties make the material a prime choice for many applications. For example, its chemical and physical properties are exploited in the field of silicon-on-sapphire devices and gallium nitride light emitting diodes (LEDs) [2–5]. For its transparency and hardness, sapphire is utilized in smartphones or watches [6–8], and for its optical properties it is also suitable for applications in the field of photonics [9, 10]. Moreover, several studies have demonstrated the possibility of producing microchannels and larger structures inside sapphire to be used for possible hosting of chemicals and chemical reactions for microfluidic applications [11–15].

Crystalline sapphire can be processed using several techniques. Typical one-step processing methods are: mechanical sawing/dicing [7, 16], dry etching [17–20], wet etching [21–23] and laser surface treatment [24–26]. Although all of the cited methods have been demonstrated to be effective, they have in common that material can only be removed starting from the surface towards the bulk. This is limiting the type of shapes/patterns achievable.

Some processing methods can be combined, yielding two-step methods [8, 11–14, 27–30]. In this paper, we present and discuss a two-step processing technique to make microstructures in the bulk and on the surface of sapphire substrates, which consists of femtosecond infrared laser irradiation to locally amorphize the material, followed by removal of the amorphized sapphire and anisotropic etching of crystalline sapphire by a mixture of sulphuric acid and phosphoric acid at a temperature of 180 °C.

When ultra-short laser pulses (in the range of femtoseconds to picoseconds) are focused inside the bulk of sapphire, the absorbed laser energy [31] induces a micro/nano explosion which creates an amorphous (or partially amorphous) [29] voxel inside the crystalline sapphire. The amorphous material can be etched selectively using specific etchants like hydrofluoric acid (HF) [11–14, 27–29] and potassium hydroxide (KOH) [32]. The most used etchant for this purpose is HF due to its high selectivity for the amorphized sapphire, having an etching rate for amorphous Al_2O_3 10^5 times higher than the etching rate for crystalline Al_2O_3. However, despite the high selectivity, which in principle should guarantee high-resolution processing of the material, several issues may arise using HF [13]. As an example, the laser amorphization of sapphire is often not carried out completely and, as a consequence, after laser irradiation, the modified material exhibits discontinuities or irregular shapes [11]. The high selectivity of HF for the amorphous phase implies that, after the etching, the empty (i.e. hollow) structure that remains has the same shape (contour/perimeter) as the amorphized material present before the etching. This obviously entails that it is not possible to modify (and improve) the shape of the structures during the etching phase.

In this work, after laser irradiation, sapphire is etched in a mixture of sulphuric acid and phosphoric acid (96 vol% H_2SO_4: 85 vol% H_3PO_4, 3:1 vol%) at 180 °C. This etchant not only rapidly dissolves the amorphized sapphire, but also anisotropically etches the crystalline sapphire. The laser-induced modifications are used as origin point to produce uniquely shaped structures inside the bulk and/or on the surface of sapphire. To the best of our knowledge, until now, laser-induced structures have never been used before as guide for anisotropic wet etching of sapphire, and particularly for laser-affected volumes in the bulk.

The mixture of H_2SO_4 and H_3PO_4 shows a higher etching rate towards the amorphized Al_2O_3 and lower selectivity compared to conventional etchants for laser-modified sapphire (e.g. HF), but it also etches crystalline sapphire anisotropically. As a consequence, in contrast to what occurs when employing HF, the crystalline material is shaped during wet etching. In this work, we exploit the latter effect to further modify the initial shape of the laser irradiated structures. In fact, the laser modified material is used as a (selective) starting point to make microstructures terminated by the slowest etching planes of crystalline sapphire. This study presents structures created in the bulk and on the surface of the substrate as a function of laser process and etching parameters.

2. Crystallographic structure and anisotropic etching of sapphire

Crystalline sapphire is a material of the trigonal crystal system with a rhombohedral lattice, and has five main crystal planes, i.e. C-, M-, A-, N- and R-planes, see figure 1(a) [1]. Anisotropic etching is a crystal orientation dependent etching method (also referred to as ODE [33–37]) in which etchants chemically react with crystalline material, with a faster etching rate along specific crystal planes compared to other planes. A variety of unique microstructures can be made with ODE having specific geometric characteristics such as sharp corners or flat surfaces. Some of the main applications of anisotropic etching are surface-texturing of sapphire [38–47], micro/nano-structuring of crystalline silicon [34, 48], or processing of crystalline quartz [49]. Anisotropic etching is also used for highlighting surface or subsurface defects of a single crystal material [50], or to understand the crystallographic structure and symmetry. When in contact with an acid, in fact, crystalline material undergoes a phenomenon called decrystallization in which the crystalline structure is broken down and this phenomenon typically starts from the discontinuities of the exposed surfaces [51]. In case of anisotropic etching of crystalline sapphire, differences in the etching rates of (main) crystal planes appear to be related to the atomic arrangement [52]. The anisotropic etchant used in this study, a mixture of sulphuric and phosphoric acid, is selected for its known property of etching sapphire anisotropically [53], by means of which crystallographically determined structures can be created on/in sapphire.

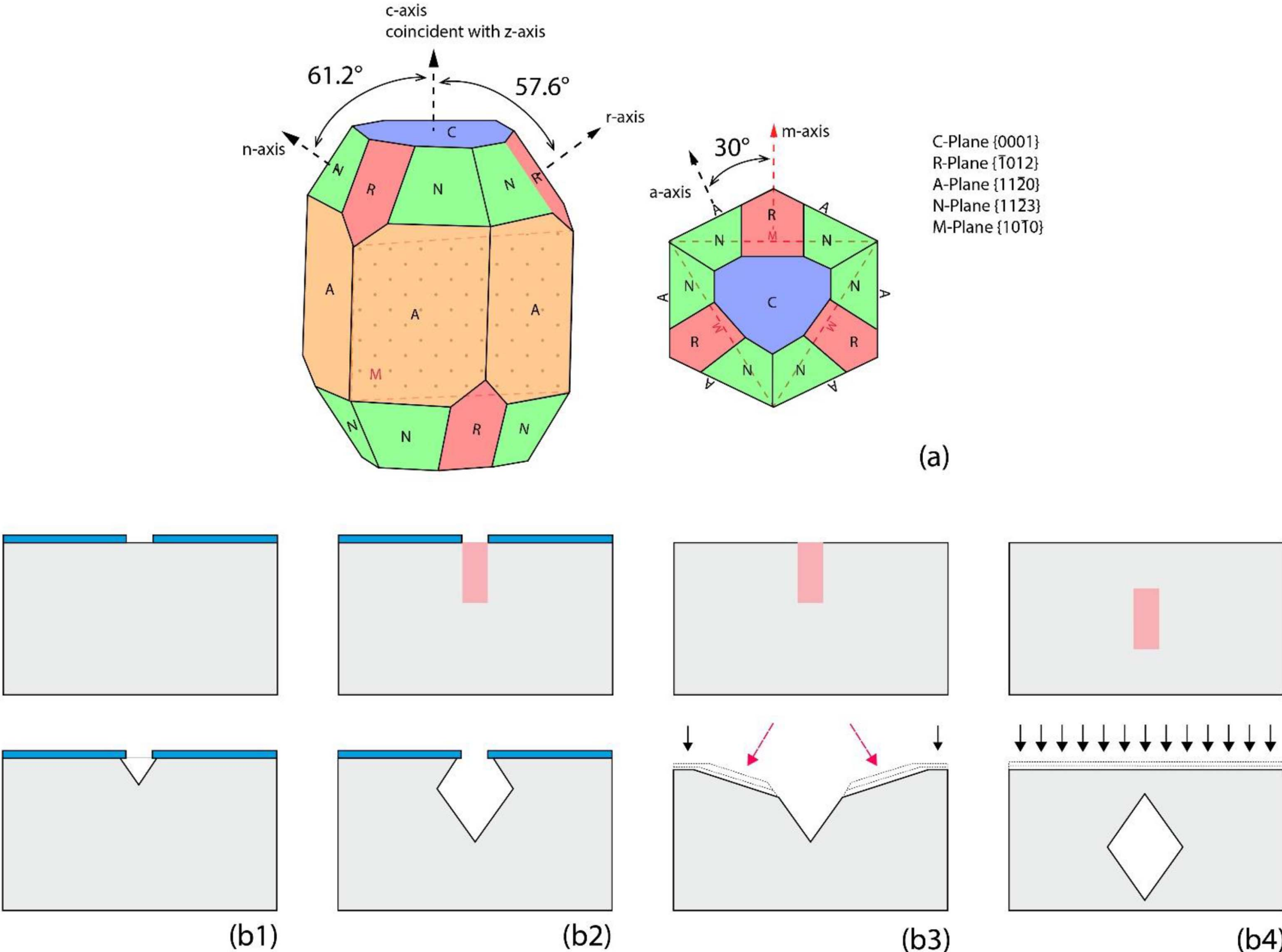

Figure 1. (a) 3D model (left) and top view (right) of the crystallographic diagram of sapphire showing the main crystal planes. (b) Schematics depicting features and processes seen in anisotropic etching of sapphire (the red areas in (b2), (b3) and (b4) are laser modified spots): (b1) concave corner etching of a masked surface, (b2) concave corner etching of a masked surface containing a modified spot, (b3) a combination of concave and convex corner etching of an unmasked surface containing a modified spot, (b4) concave corner etching of a subsurface located modified spot.

Aota *et al* [38] discussed the main etching mechanisms of anisotropic etching of sapphire when using this mixture for surface-texturing of substrates. They analyzed the etching of sapphire in the mixture as well as in each of the acids composing the solution and found that sulphuric acid has a higher etching rate towards the crystalline sapphire than phosphoric acid. However, etching of the material in solely sulphuric acid produces a precipitate ($Al_2(SO_4)_3$) which deposits on the surface and prevents further etching. Furthermore, they showed that an elevated temperature of the mixture results in an increase of the etching rate. Using this knowledge, Aota *et al* textured the surface of sapphire by means of anisotropic etching in a mixture of phosphoric and sulphuric acid in combination with a (patterned) hard mask of silicon dioxide SiO_2 [38, 39]. This process is schematically shown in figure 1(b1): the etched concave features are confined by the slowest etching crystal planes. In fact, the crystallographic facets terminating a structure anisotropically etched in sapphire depend on (a) whether (or not) a hard mask was present on the surface of the substrate during etching and (b) whether (or not) the surface contained spots at which the crystalline structure was modified (e.g. laser irradiated areas). The presence of a patterned mask layer results in concave corner etching (figures 1(b1) and (b2)), regardless of the presence/absence of laser irradiated spots/areas on the surface. Concave corner anisotropic etching is obtained if the surface of the substrate is protected (for example by a hard mask) and inhibits convex corner anisotropic etching on rims and edges [48, 53]. If no hard mask is present, the (flat) surface of sapphire etches uniformly, as indicated by the black arrows in figure 1(b3)). Moreover, the absence of a hard mask results in convex corner etching at the top of laser modified spots and therefore the appearance of fast etching crystal planes (as indicated by the red dashed arrows in figure 1(b3)), as well as concave corner etching in deeper regions of the non-crystalline areas. In contrast, if the irradiated areas are located in the bulk of the sapphire (i.e. subsurface) only concave corner etching occurs (figure 1(b4); it is noted that the latter is investigated in detail in this work). The difference between 'concave corner anisotropic etching' and 'convex corner anisotropic etching' lays in the crystallographic planes revealed in the structures

Table 1. Etching rates for crystalline and amorphized sapphire for the investigated anisotropic etchant (mixture of sulphuric acid and phosphoric acid (3:1 vol%) at 180 °C).

Type of sapphire	Etching rate (nm min^{-1})
C-plane	1.2
R-plane	0.1
Amorphized	532.1

after wet etching (see figure 1(b)). Whereas Aota *et al* [38] textured the surface of sapphire with concave anisotropic etching, Shen *et al* [40, 41] applied convex anisotropic etching to cylindrical pillars of sapphire to fabricate cone-shaped patterned sapphire substrates (PSS). In this paper, laser treated areas (on the surface and in the bulk) are exposed to anisotropic etching. This implies that for all the investigated specimens both concave and convex etching occur simultaneously. The etching rates in the mixture (of H_2SO_4 and H_3PO_4) at 180 °C were found experimentally for the C-plane and R-plane of crystalline sapphire as well as for amorphized sapphire. The found etching rates, in nm min^{-1}, are shown in table 1. Please refer to section 3.3 for a detailed description of the methods employed for measuring the etching rates.

3. Materials and methods

3.1. Materials

Three types of substrates were used for the experiments. The first type was a circular 2-inch wafer (Crystec, Germany) with a thickness of 430 μm oriented along the *C*-axis (0001), the second was a circular 4-inch wafer (Kyocera, Japan) with a thickness of 630 μm oriented along the *C*-axis (0001), and the third was a circular 2-inch wafer (Crystec, Germany) with a thickness of 430 μm oriented along the *R* axis. All of the laser irradiation experiments were conducted on the 2-inch wafers oriented along the *C*-axis (Crystec). The other wafers were used only for the determination of the etching rate for C- and R-planes.

The chemical etchant used is a stagnant solution of 96% H_2SO_4 + 85% H_3PO_4 (vol%) in volumes respectively of 2850 ml and 950 ml (ratio of 3:1). The etchant solution was heated to a temperature of 180 °C. This temperature was chosen because it is the highest that the solution may reach before producing highly toxic fumes that are difficult to handle in this etching setup. Since the etching bath is a closed system and considering the fact that the volume of etching biproducts is negligible with respect to the volume of the solution, the concentration of the mixture can be considered constant at all the time steps.

3.2. Laser set-up

The laser set-up that was used to tightly focus laser pulses on the surface and inside crystalline sapphire is shown in figure 2. The laser source used for this study is a fiber laser (Y-Fi, KMLabs, USA) emitting a linearly polarized beam at a central wavelength of λ = 1035 nm. It has a full width at

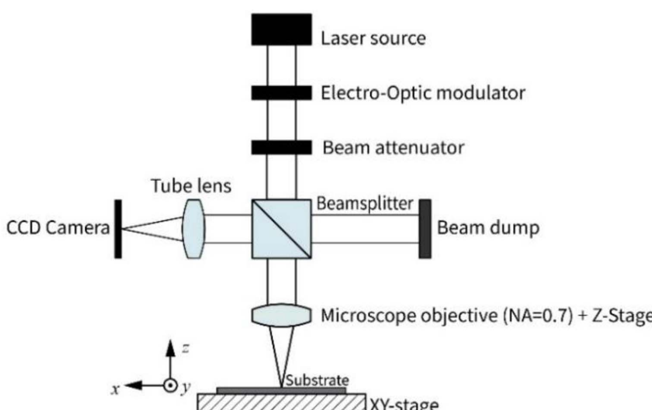

Figure 2. Laser set-up used in this study.

half maximum pulse duration of 230 fs (measured with the autocorrelator 'pulse-Check' by APE-Berlin, Germany). The spatial beam profile of the beam is nearly Gaussian with a beam quality M^2 < 1.2. The repetition rate of the pulses is controlled by an electro-optic modulator (360-80, Conoptics, USA) and the pulse energy is set with a beam attenuator (Ultrafast Version, Altechna, Lithuania).

The microscope objective employed (model 11101666, Leica Microsystems, Germany) has a numerical aperture (NA) of 0.7 and focuses the laser beam to a diameter of about 0.9 μm (calculated). The same lens is used also for monitoring the process and to position the focal spot on the surface or inside the substrate. To that end, a beam splitter is used to redirect the light which is reflected back from the specimen to a camera (DCC1545, Thorlabs, USA) through a tube lens.

The objective is moved along the *z*-axis (focusing axis) using a linear stage (ATS100, Aerotech, USA, resolution 100 nm) allowing the positioning of the focus spot on top of the surface or inside the bulk of the material. The computerized mechanical stages (*X* and *Y* axes) used to move the substrate during laser processing, are ALS 130-150 (Aerotech, USA) with a resolution of 50 nm.

3.3. Methods

For the experiments, simple structures were produced on the surface and in the bulk of the sample to study the influence of experimental laser parameters on the process of laser modification and selective anisotropic etching. To produce such structures, the sample is moved with a constant velocity while the substrate is exposed to laser pulses emitted by the laser source.

The geometrical pulse-to-pulse overlap (OL) in percent mentioned in the paper is defined here as [11, 53] (equation (1))

$$\mathrm{OL} = [1 - (v/f \cdot D)] \times 100 \quad (1)$$

where v is the relative velocity between the laser beam and the substrate, D is the diameter of the laser spot in the focus and f is laser pulse repetition rate. By changing the velocity (in the x- or y-direction as shown in figure 2) and the pulse repetition rate, the pulse-to-pulse OL is varied and either

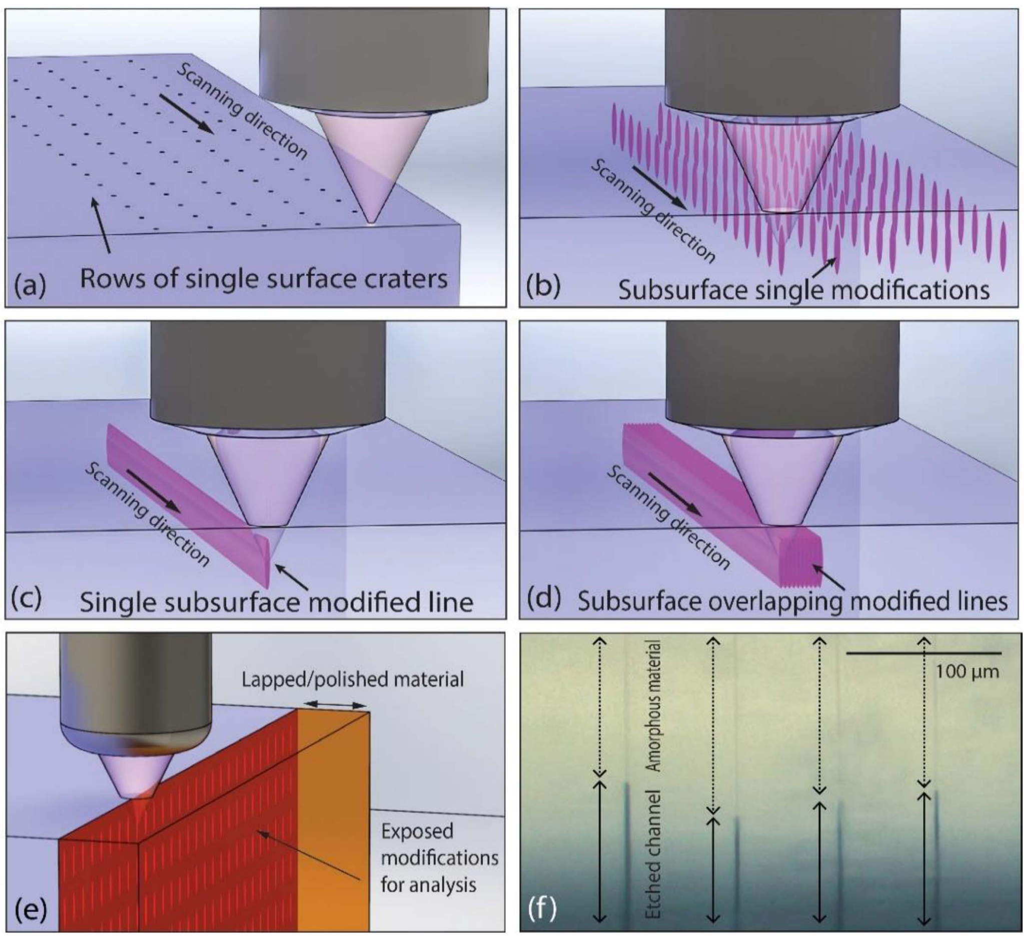

Figure 3. Schematic representation of the various types of laser-induced structures produced and analyzed in this study: (a) single craters on the surface of the sample; (b) single isolated modifications 30 μm below the surface of the sample; (c) single laser-modified lines made of overlapping laser pulses produced 30 μm below the surface of the sample; (d) larger lines produced 30 μm below the surface of the sample made by overlapping single laser-induced modified lines; (e) to expose cross-sections of the modifications, the substrate is lapped and polished, following laser processing, to remove the bulk material (orange); (f) optical microscopy image (top view) of channels obtained after irradiation and etching in the anisotropic mixture for about 364 min. The etching rate is calculated by measuring the etched channel lengths at different time steps.

single, separated, modifications (figures 3(a) and (b)) or lines resulting from the overlapping modifications (figures 3(c) and (d)) are produced. The focus is positioned either on the surface of the sample (figure 3(a)) or at a processing depth of 30 μm below (figures 3(b)–(d)), by moving the microscope objective (attached to the z-stage, see figure 2). The processing depth, the energy per laser pulse and the pulse repetition rate were selected based on our earlier work [11]. All the laser-induced modifications are produced close to (about 5 mm) the margins of the substrate for easy access. After the laser irradiation, the samples are lapped and polished (figure 3(e)) using a Tegramin polishing machine (Struers, USA) to expose the cross-sections of the modified material. The 2-inch wafers were lapped and polished in a direction such that the polished face is approximately parallel to the wafer flat (A-plane). The surface roughness after the last step of polishing is $R_a < 5$ nm. This surface quality allows an easy characterization of the cross-sections. After polishing, the samples are cleaned in an ultrasonic isopropanol bath. Subsequently, etching is carried out by submerging the substrate in the stagnant solution in three subsequent rounds: 364 min, 385 min (749 in total), 364 min (1113 in total). The etching periods reported in the figures indicate the cumulative etching time at each step. After etching, the substrates are cleaned again with deionized (DI) water with a quick dump rinse process. The etching rates for C- and R-planes listed in section 2 were calculated by etching C-type and R-type sapphire specimens in the mixture of phosphoric and sulphuric acid. These samples were covered with a patterned SiO_2 mask of 1080 nm (deposited using plasma-enhanced chemical vapor deposition in an Oxford 80 system (parameters: 300 °C, 650 mTorr, 200 sccm SiH_4, 719 sccm N_2O, time: 30 min)) which had areas (created by standard UV-lithography (photoresist: Olin 907-17, FujiFilm), selective SiO_2 removal with buffered hydrofluoric acid (BASF, time: 10 min) and removal of photoresist with acetone (BASF)) for locally exposing the surface of the sapphire specimen to the acid mixture. The etching rates of C- and R-planes were calculated by measuring the depth of the exposed sapphire areas after 1092 min etching. For amorphized sapphire, the etching rate was calculated by measuring the length of the etched

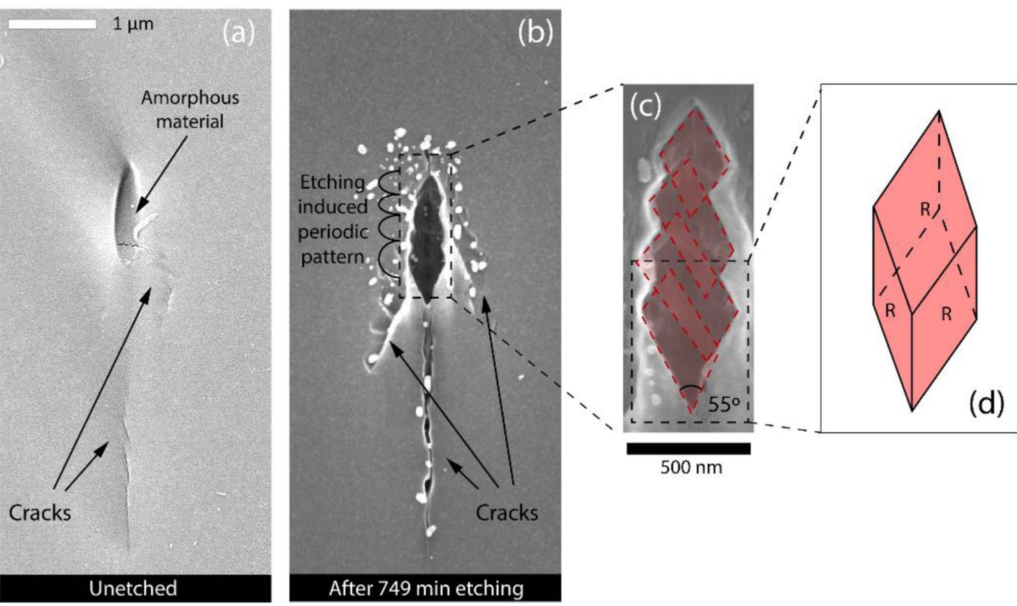

Figure 4. SEM micrographs of a typical cross-section of (a) a single-laser pulse induced modification after laser irradiation, (b) after 749 min etching in the mixture of H_2SO_4 and H_3PO_4 at 180 °C. A laser pulse energy of 94.5 nJ was used and the direction of the laser beam was from top to bottom in the micrographs. The C-plane is parallel to the horizontal direction of the images. Anisotropic etching causes (c) periodic structures bounded by R-planes (d) 3D representation of the rhombohedron formed by the R-planes of the sapphire crystal as the unit cells of the periodic patterns. It is noted that the SEM-images in (a) and (b) are on the same scale (scale bar in (a) valid for (b)).

amorphized part for the same channels used for the study of the cross-sections (figure 3(f)). In this case, the measurements were performed via optical microscope by observing the top view of the channels (the etched part appears darker) after the same etching steps as the cross-sectional analysis.

3.4. Analysis tools

The analysis of the specimen after laser irradiation is performed with a high resolution scanning electron microscope (SEM; JEOL7200F, Japan). The same substrates are analyzed at identical positions before and after each etching step. Height profiles of the surface were obtained using a S-Neox (Sensofar Metrology, Spain) confocal microscope and a FlexAFM (Nanosurf AG, Switzerland) atomic force microscope.

4. Results and discussion

The main objective of this research is to study a processing technique based on selective and anisotropic etching, using a mixture of H_2SO_4 and H_3PO_4 at 180 °C, of laser-treated sapphire. This paper shows results regarding the etching behavior for both surface and subsurface (bulk) laser-induced structures.

4.1. Subsurface processing

4.1.1. Single-pulse-induced bulk modifications. Single-laser-pulse-induced modifications were produced at about 30 μm below the surface, by exposing the specimen to laser pulses at a repetition rate of 1 kHz while moving the sapphire substrate at a velocity of $v = 15$ mm s^{-1} (corresponding to an inter-pulse distance of about 15 μm). In figure 4, a cross-section of a typical modification induced by a single laser pulse is shown. The horizontal direction of the SEM micrographs is oriented parallel to the C-plane (<2°, estimated by comparing the horizontal direction in the frontal appearance of the micrographs with the top surface of the sample, which, in turn, is oriented parallel to the C-plane). It has to be noted that the areas surrounding modified spots remain unaffected by the laser/etch process. The amorphized volumes of Al_2O_3 in the SEM micrograph of the cross-section before the etching (figure 4(a)) appears darker than the crystalline sapphire surrounding the modification. As can be observed from figure 4(b), etching the single modifications causes an etching-induced periodic pattern. This type of pattern consists of repeated regular 3D shapes along the length of the single-pulse-induced structure (figure 4(c)). Our assumption for the formation of the pattern is that the R-planes, which have an inclination of 57° with respect to the C-plane (figure 1(a)), terminate the etched structures. The intersection of the six R-planes form all together a rhombohedron (figure 4(d)). This is assumably the shape of the single feature composing the periodic pattern (the angle of 55° measured at the base of the modification is reasonably close to the 57° angle between the R-plane and the C-plane).

In figure 5 two sets of SEM micrographs are shown: the first set (figures 5(a)–(d)) shows single-pulse induced modifications made using a pulse energy of 94.5 nJ; the second set (figures 5(e)–(h)) is made at a higher pulse energy of 457 nJ. The region of amorphized sapphire is discernible in figures 5(a) and (e) (unetched). The evolution of the visual cross-sectional appearance with etching time is similar for both the pulse energies shown. The dimensions of the etching

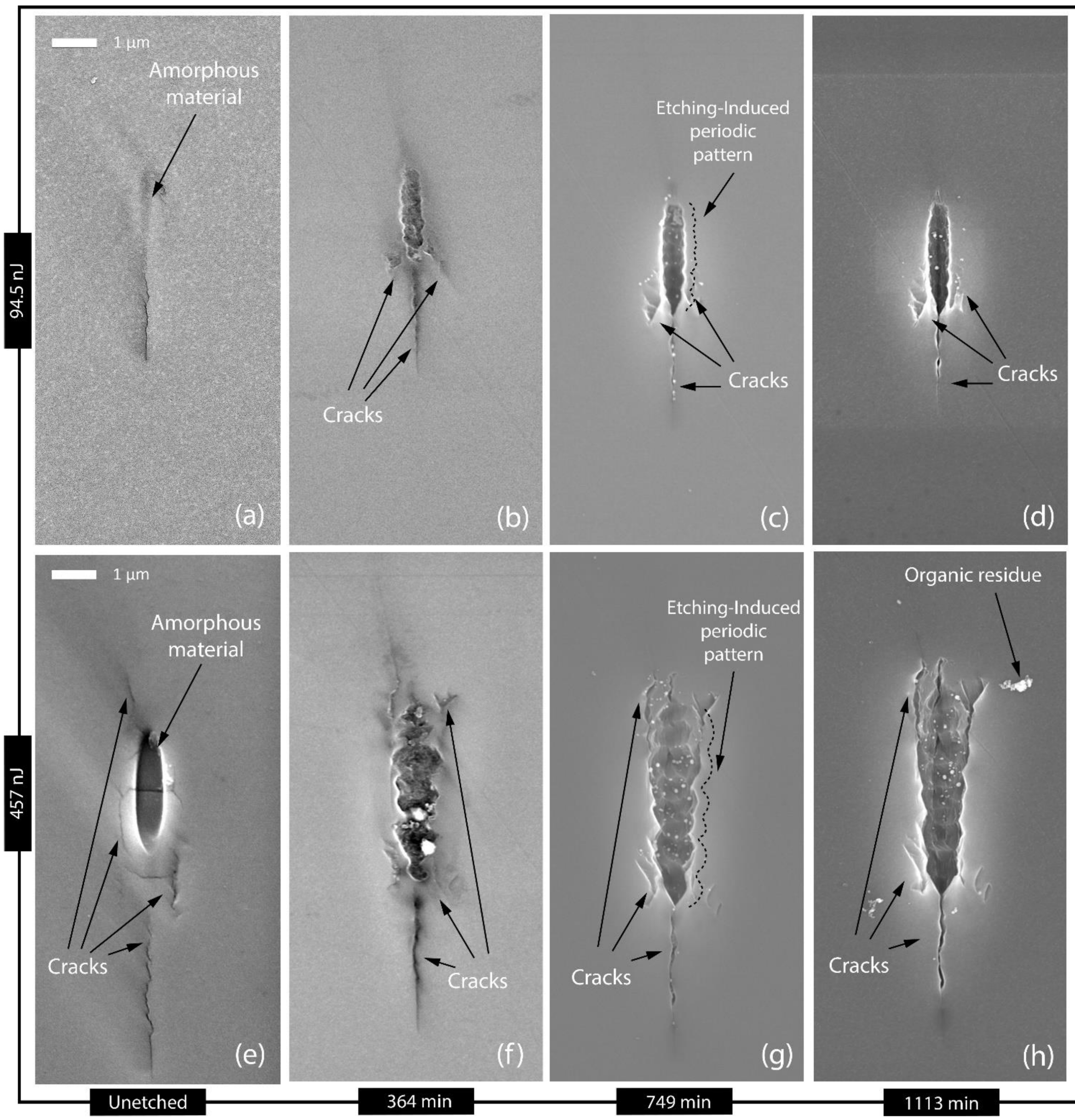

Figure 5. SEM micrographs of cross-sections (a), (e) after irradiation and ((b)–(d), (f)–(h)) after etching of single-laser-pulse-induced modifications obtained positioning the focal spot of the laser beam 30 μm below the surface and using the pulse energies: 94.5 nJ (top row) and 457 nJ (bottom row). The direction of the laser beam was from top to bottom. It is noted that all SEM-images are on the same scale (scale bar in (a) and (e) valid for all images).

induced structures, as expected, increase with a higher energy per pulse. Cracks, which are typical for this type of process [29], are higher in number and larger in size for the pulse energy of 457 nJ compared to 94.5 nJ. As can be observed from figure 5, the amorphous material, which looks darker than the surroundings in the SEM micrographs, is fully removed after 364 min and the etching-induced patterns are visible throughout the etching process (figures 5(b)–(d) and (f)–(h)). Also, the crystalline material surrounding the modified material is etched anisotropically and the resulting modification is widened, as can be observed most clearly after 1113 min of etching (figures 5(d) and (h)). The latter can be explained by convex etching of the rims of the cracks exposing fast etching planes (see figure 1(b3)).

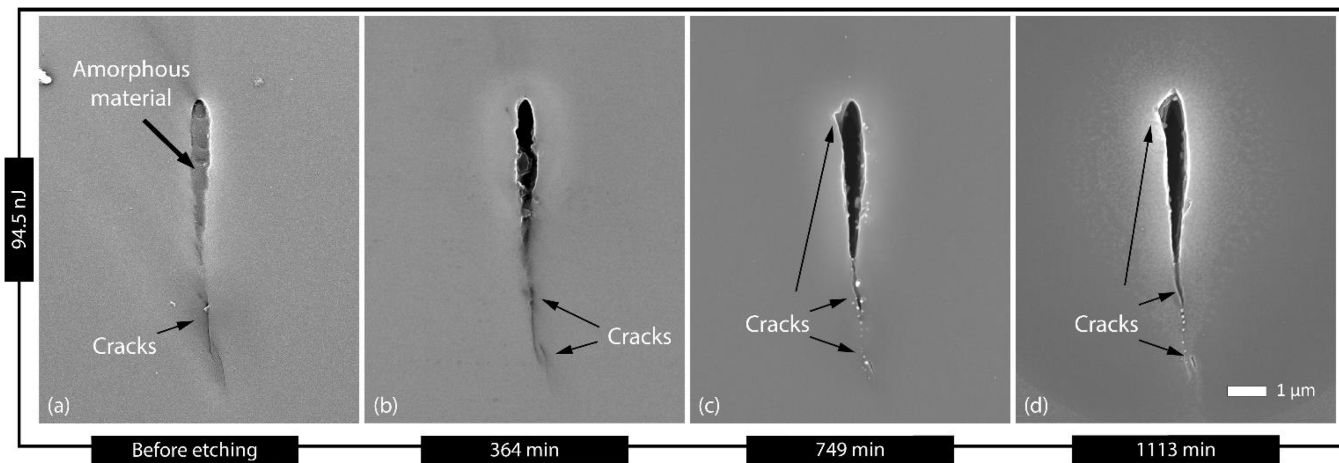

Figure 6. SEM micrographs of cross-sections (a) after irradiation and (b)–(d) after etching of irradiated lines produced positioning the focal spot of the laser 30 μm below the surface of the sample using a pulse energy of 94.5 nJ, a pulse repetition rate of 200 kHz and a stage velocity of 1 mm s^{-1}. The direction of the laser beam was from top to bottom. It is noted that all SEM-images are on the same scale (scale bar in (d) valid for all images).

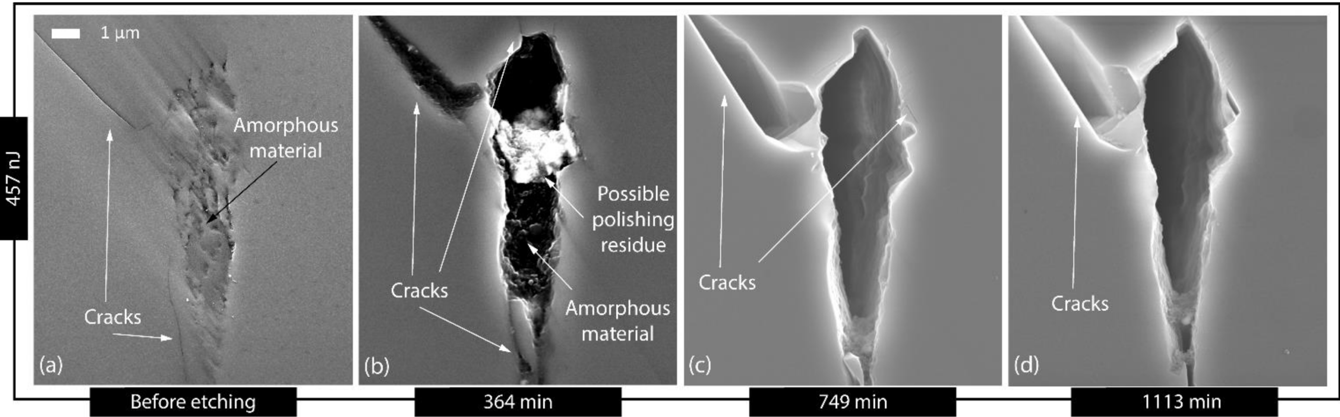

Figure 7. SEM micrographs of cross-sections (a) after irradiation and after 364, 749 and 1113 min of etching (b)–(d) of a large structure produced by laterally overlapping eight irradiated lines. The structure was produced positioning the focal spot of the laser 30 μm below the surface of the sample, using a pulse energy of 457 nJ, a pulse repetition rate of 200 kHz and a stage velocity of 1 mm s^{-1}. The direction of the laser beam was from top to bottom. It is noted that all SEM-images are on the same scale (scale bar in (a) valid for all images); in (b) possibly some polishing residue is visible.

4.1.2. Subsurface microchannels and large structures. Subsurface channels were produced using the method described in section 3.3. Figure 6 shows the cross-section of a channel produced using a pulse energy of 94.5 nJ, a pulse repetition rate of 200 kHz and a stage velocity v = 1 mm s^{-1} (corresponding to a pulse-to-pulse OL of 99.99%), at varying etching times. As can be observed from figure 6, the obtained channels closely resemble those obtained in our earlier work [11] using stagnant HF (50%) at room temperature as etchant. However, a difference with respect to HF as etchant is the contour of the cross-section after using the anisotropic mixture. The anisotropic etching 'smoothens' the perimeter of the etched channel (figure 6(d)). In case of HF, the rough, irregular contour was only due to the laser irradiation (and not due to HF-etching of the crystalline material). Similarly to the case of single-laser-pulse-induced modifications, cracks are subject to anisotropic etching, which proceeds along the crack direction.

Figure 7 shows SEM micrographs of the evolution of a cross-section as a function of etching time for a structure produced using a pulse energy of 457 nJ, a pulse repetition rate of 200 kHz, at 30 μm below the surface of the substrate and by overlapping (laterally, side by side) eight modified lines at a distance of 50 nm to each other to form a larger structure: over time, the structure enlarges. Moreover, the cracks surrounding the structure are affected by the anisotropic etchant. In particular, as evident in figures 5(d), 6(d) and 7(d), the convex anisotropic etching has the general effect of widening the cracks.

4.2. Surface processing

Single laser-induced craters (figure 8(a)) were produced on the surface of a sapphire specimen with a method similar to the method described in section 4.1.1. The stages were moved at a speed of 15 mm s^{-1} while laser pulses were emitted with a repetition rate of 1 kHz using a laser pulse energy of

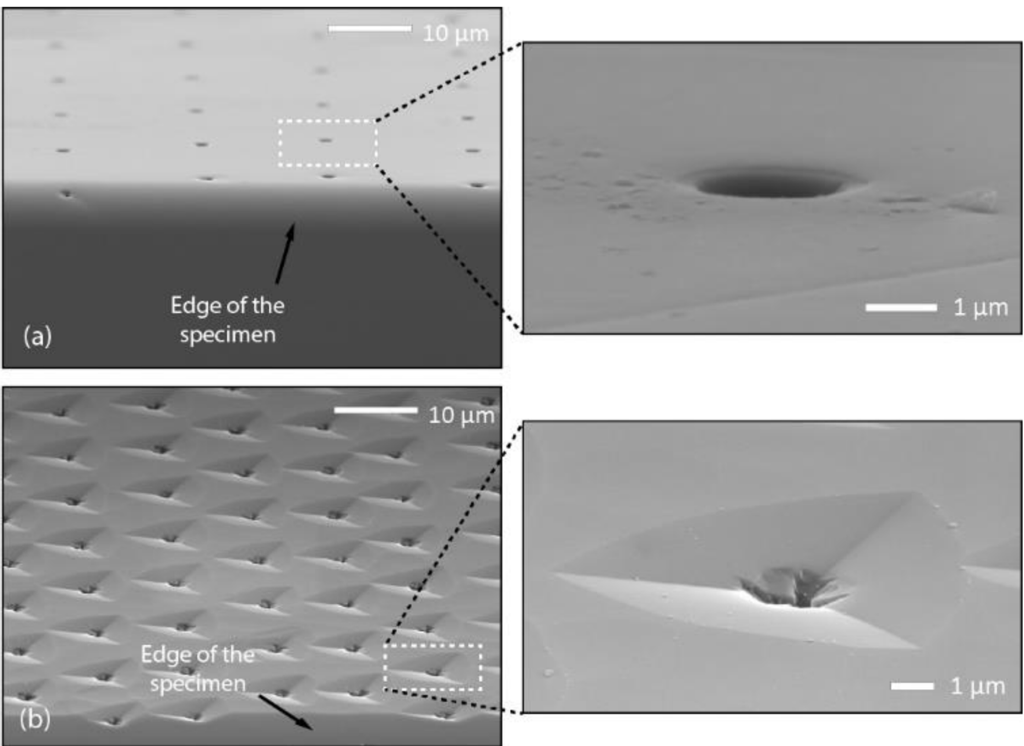

Figure 8. SEM micrographs of a pattern of single-pulse induced modifications (a) (30° tilted view) before etching and (b) (60° tilted view) after 749 min etching, produced on the surface of the sample using a pulse energy of 94.5 nJ.

94.5 nJ. The focal spot was positioned on the surface of the sample. Different from the laser-induced bulk modifications, the craters on the surface are mainly formed by laser ablation of the material [54] rather than by amorphization. This implies that the mechanism driving the etching of these craters is different. We think that, during immersion of the surface-irradiated sapphire specimen in the wet chemical etchant mixture, etching of the crystalline sapphire is initiated at the edge of the ablated crater and occurs by monolayer steps running outward from the damaged region at a specific step flow rate that creates three planes at a relatively low angle with the top surface of the specimen (figure 8(b)). These features look quite similar to what has been observed on Si {111} surfaces during anisotropic etching, where it was proven that the triangular pits initiate from crystal dislocations [55]. The formed triangular shapes can have straight or curved periphery, which for Si {111} has been interpreted as a result of step curvature, which is determined by the relative removal rates of atoms at step and kink positions [56]. Our pits clearly show a curved periphery.

Figure 9(a) shows a height profile of the surface obtained by confocal microscopy, after 1113 min of anisotropic etching. An array of triangular pits can be seen. The surface-edge angle of the pits was found to be 5.3° ± 0.3°, whilst the face of the triangular pits shows an angle of 8.5° ± 0.1° with respect to the substrate surface of the substrate. As the confocal microscope did not have sufficient resolution for the center of the pits (see the central part of the graph in figure 9(a)), atomic force microscopy (AFM) was performed for inspection of the central structure. Figure 9(b) shows a height profile of a single pit, obtained with AFM after 1113 min of etching. The depth at the center of the pit is about 0.9 μm. As mentioned above, the low angles on the outer side of the structures can be explained by step flow starting from the central defective region of the pit.

This hypothesis differs from the reasoning of Aota *et al* [38], who state that the observed structures might be the effect of the deposition of reaction products on the surface. In fact, in their study Aota *et al* suggest that the stable $\left\{10\bar{1}\bar{1}k\right\}$ planes that would theoretically terminate the surface modifications are masked by the redeposited material, leading to the shallow inclination of the faces.

In figure 10 the evolution over time of the shapes can be seen after various etching periods. Figure 10(a) shows a top view of a typical laser ablated crater. The shape of the crater roughly equals the shape of the Gaussian fluence profile of the laser spot. Before assuming the final triangular shape, after the first etching period (364 min, figure 10(b)), the structure shows more than three faces. Superimposed on this shape, a hexagonal shape forms in the center of the structure. The latter is caused by the fact that the plane parallel to the C-plane (parallel to the surface of the specimen), etches faster than the other planes in the used anisotropic etchant. This results in a 'hole' in the sample and its edges have an hexagonal shape because of the lower etching speed for those planes parallel to the faces of the hexagon. In this case, the hexagonal shape and the faces perpendicular to the C-plane, suggest that A-planes (figure 1(a)) define the shape of the hole. After 749 min of etching (figure 10(c)), the additional planes disappear and a triangular (top view) shape rotated about 90° forms in the center. After 1113 min (figure 10(d)) a three-armed cross-shaped

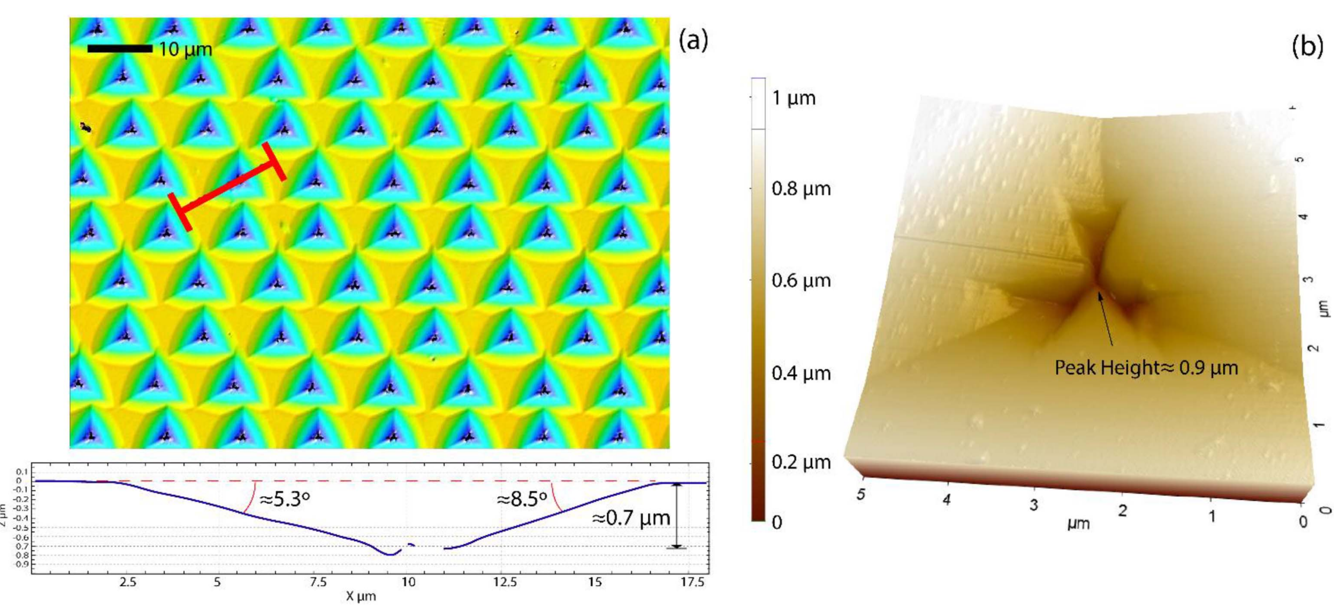

Figure 9. (a) Top: confocal microscopy image of an array of single laser-pulse induced craters after 1113 min etching. Bottom: profile of an etched crater along the edge and the face of the triangular pit. The scan is performed along the red line in the figure. (b) Height profile of the central area of a crater obtained by atomic force microscopy.

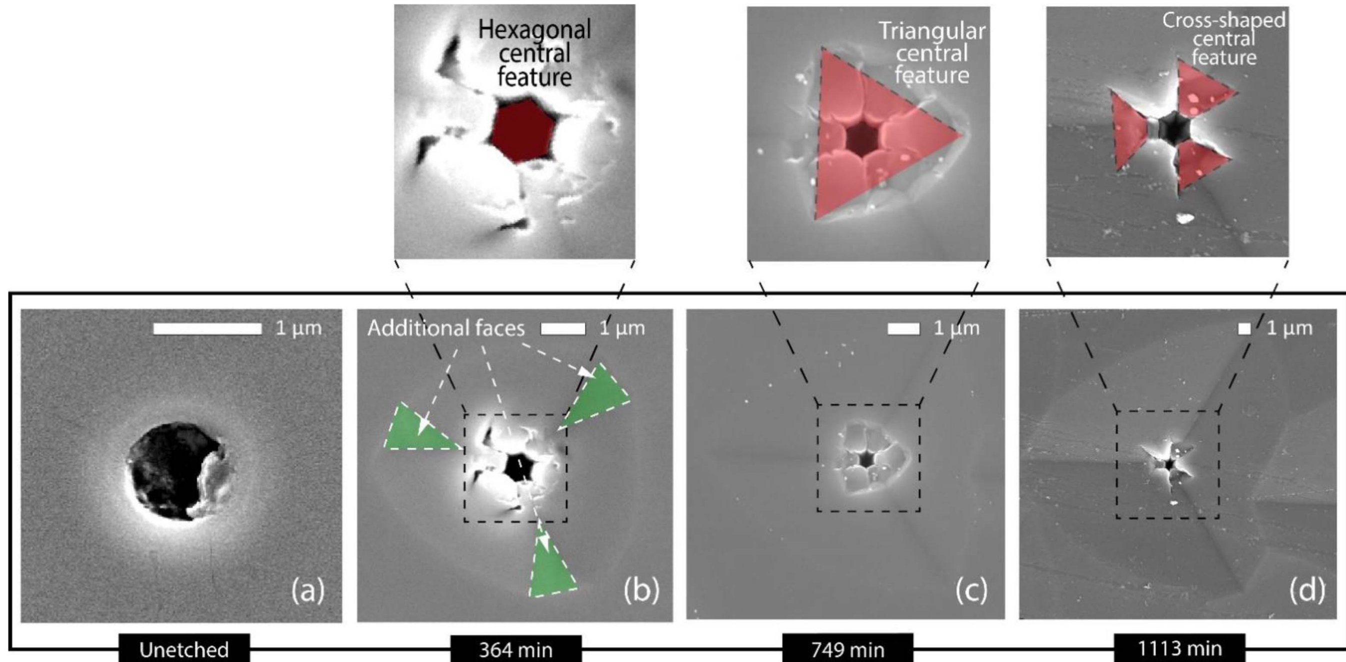

Figure 10. SEM micrographs (top view) of a single-laser pulse induced crater on the surface (a) after laser-irradiation and (b)–(d) after etching (craters formed by moving the substrate with a velocity of 15 mm s^{-1}, a pulse repetition rate of 1 kHz and a pulse energy of 94.5 nJ). The top row shows details of the intermediate structures forming at each etching step in the center of the craters.

structure evolves in the center. An AFM measurement of this shape is shown in figure 9(b).

5. Conclusions

A study has been performed on a two-step fabrication technique which combines laser modification of sapphire with selective wet etching of locally amorphized sapphire and anisotropic wet etching of crystalline sapphire (α-Al_2O_3). Different types of structures have been produced on the surface and in the bulk of sapphire and were analyzed before etching as well as after several etching time steps.

The first part of the investigation focused on subsurface single-pulse induced structures. After the complete dissolution of the amorphized part, anisotropic etching of the crystalline sapphire yielded structures with an etching-induced periodic pattern. The facets of the pattern are defined by the R-planes of

the sapphire crystal, resulting in an arrangement with repeating rhombohedra. Subsequently, subsurface modified lines were studied. Single lines and large structures (made by laterally overlapping of single lines) were produced below the surface with high pulse-to-pulse OL. The resulting structures after etching in the anisotropic etchant showed, in general, identical cross-sections as the ones obtained in our previous work using an isotropic etchant (in which crystalline sapphire is hardly etched). However, the contour of the hollow structures shows less roughness and irregularities, which is caused by anisotropic etching of the crystalline material exposing the slow etching R-planes. The cracks in the crystalline material surrounding the modifications were also etched and their shape was widened. Next, in order to investigate the surface structures, single-laser-pulse-induced structures (craters) were produced on the surface of the sample. Anisotropic etching of such structures produced triangular pits. The reason for such shape was found in the step flow etching of the single surface craters.

The results of this study suggest that a higher etching time or etching rate can lead to the formation of subsurface structures having highly smooth walls. Such structures could find good use for microfluidic applications. Finally, having specific orientations, the surface structures shown in this paper could be used for surface texturing and tribological applications.

Data availability statement

The data that support the findings of this study are available upon reasonable request from the authors.

Acknowledgments

Dr L Chu (Surface Technology & Tribology group and Production Technology group of University of Twente) is acknowledged for performing the Atomic Force Microscopy measurements.

Funding

The project Laser4Fun (www.laser4fun.eu) leading to this article has received funding from the European Union's Horizon 2020 research and innovation programme under the Marie Skłodowska-Curie Grant Agreement No. 675063.

ORCID iDs

L Capuano https://orcid.org/0000-0001-6126-725X
J W Berenschot https://orcid.org/0000-0002-4721-2997
R M Tiggelaar https://orcid.org/0000-0002-4021-5036
M Feinaeugle https://orcid.org/0000-0002-4721-2997
N R Tas https://orcid.org/0000-0001-7541-4345
J G E Gardeniers https://orcid.org/0000-0003-0581-2668
G R B E Römer https://orcid.org/0000-0002-4721-2997

References

[1] Dobrovinskaya E R, Lytvynov L A and Pishchik V 2009 *Sapphire: Material, Manufacturing, Applications* (Heidelberg: Springer) (https://doi.org/10.1007/978-0-387-85695-7)

[2] Kitamura S, Hiramatsu K and Sawaki N 1995 Fabrication of GaN hexagonal pyramids on dot-patterned GaN/sapphire substrates via selective metalorganic vapor phase epitaxy *Jpn. J. Appl. Phys.* **34** L1184–6

[3] Li K H, Cheung Y F, Fu W Y, Wong K K Y and Choi H W 2018 Monolithic integration of GaN-on-sapphire light-emitting diodes, photodetectors, and waveguides *IEEE J. Sel. Top. Quantum Electron.* **24** 1–6

[4] Kim T-I *et al* 2012 High-efficiency, microscale GaN light-emitting diodes and their thermal properties on unusual substrates *Small* **8** 1643–9

[5] Reklaitis I, Grinys T, Tomašiunas R, Puodžiunas T, Mažule L, Sirutkaitis V, Lin C H and Yang C C 2015 A new geometrical approach for rapid LED processing by using femtosecond laser *Opt. Lasers Eng.* **74** 17–21

[6] Lin G and Huang Y 2018 High mechanical strength sapphire cover lens for smartphone screen *Cryst. Res. Technol.* **53** 1800049

[7] Hayes D 1998 Sapphire watch glass machining with diamond *Ind. Diam. Rev.* **58** 55–56

[8] Kaiser M, Kumkar M, Leute R, Schmauch J, Priester R, Kleiner J, Jenne M, Flamm D and Zimmermann F 2019 Selective etching of ultrafast laser modified sapphire *Proc. SPIE* **10905** 109050F

[9] Dutta A, Kinsey N, Saha S, Guler U, Shalaev V M and Boltasseva A 2016 Plasmonic interconnects using zirconium nitride *Conf. Lasers Electro-Optics* (Optical Society of America) p JW2A-86

[10] Baehr-Jones T, Spott A, Ilic R, Spott A, Penkov B, Asher W and Hochberg M 2010 Silicon-on-sapphire integrated waveguides for the mid-infrared *Opt. Express* **18** 12127

[11] Capuano L, Tiggelaar R M, Berenschot J W, Gardeniers J G E and Römer G R B E 2020 Fabrication of millimeter-long structures in sapphire using femtosecond infrared laser pulses and selective etching *Opt. Lasers Eng.* **133** 106114

[12] Wortmann D, Gottmann J, Brandt N and Horn-Solle H 2008 Micro-and nanostructures inside sapphire by fs-laser irradiation and selective etching *Opt. InfoBase Conf. Paper* vol 16 pp 1517–22

[13] Juodkazis S, Nishimura K, Misawa H, Ebisui T, Waki R, Matsuo S and Okada T 2006 Control over the crystalline state of sapphire *Adv. Mater.* **18** 1361–4

[14] Hörstmann-Jungemann M, Gottmann J and Keggenhoff M 2010 3D-microstructuring of sapphire using fs-laser irradiation and selective etching *J. Laser Micro Nanoeng.* **5** 145–9

[15] Moser R, Ojha N, Kunzer M and Schwarz U T 2011 Sub-surface channels in sapphire made by ultraviolet picosecond laser irradiation and selective etching *Opt. Express* **19** 24738

[16] Matsumaru K, Takata A and Ishizaki K 2005 Advanced thin dicing blade for sapphire substrate *Sci. Technol. Adv. Mater.* **6** 120–2

[17] Kim B-J, Mastro M A, Jung H, Kim H-Y, Kim S H, Holm R T, Hite J, Eddy C R, Bang J and Kim J 2008 Inductively coupled plasma etching of nano-patterned sapphire for flip-chip GaN light emitting diode applications *Thin Solid Films* **516** 7744–7

[18] Hsu Y P, Chang S J, Su Y K, Sheu J K, Kuo C H, Chang C S and Shei S C 2005 ICP etching of sapphire substrates *Opt. Mater.* **27** 1171–4

[19] Jeong C H, Kim D W, Lee H Y, Kim H S, Sung Y J and Yeom G Y 2003 Sapphire etching with BCl_3/HBr/Ar plasma *Surf. Coatings Technol.* **171** 280–4

[20] Furuya H, Okada N and Tadatomo K 2012 Growth of {11-22} GaN on shallowly etched r-plane patterned sapphire substrates *Phys. Status Solidi* **9** 568–71

[21] Liu M, Hu Y, Sun X, Wang C, Zhou J, Dong X, Yin K, Chu D and Duan J 2017 Chemical etching mechanism and properties of microstructures in sapphire modified by femtosecond laser *Appl. Phys.* A **123** 99

[22] Jiang S X, Chen Z Z, Jiang X Z, Fu X X, Jiang S, Jiao Q Q, Yu T J and Zhang G Y 2015 Study on the morphology and shape control of volcano-shaped patterned sapphire substrates fabricated by imprinting and wet etching *CrystEngComm* **17** 3070–5

[23] Cuong T V, Cheong H S, Kim H G, Kim H Y, Hong C-H, Suh E K, Cho H K and Kong B H 2007 Enhanced light output from aligned micro-pit InGaN-based light emitting diodes using wet-etch sapphire patterning *Appl. Phys. Lett.* **90** 131107

[24] Nieto D, Arines J, O'Connor G M and Flores-Arias M T 2015 Single-pulse laser ablation threshold of borosilicate, fused silica, sapphire, and soda-lime glass for pulse widths of 500 fs, 10 ps, 20 ns *Appl. Opt.* **54** 8596

[25] Zhai Z, Wang F and Duan H 2019 Experimental study on 800 nm femtosecond laser cutting of polyamide in air *Optik* **194** 163080

[26] Chen T-C and Darling R B 2005 Parametric studies on pulsed near ultraviolet frequency tripled Nd: yAGlaser micromachining of sapphire and silicon *J. Mater. Process. Technol.* **169** 214–8

[27] Matsuo S, Tokumi K, Tomita T and Hashimoto S 2008 Three-dimensional residue-free volume removal inside sapphire by high-temperature etching after irradiation of femtosecond laser pulses *Laser Chem.* **2008** 892721

[28] Juodkazis S and Misawa H 2007 Forming tiny 3D structures for micro- and nanofluidics (SPIE Newsroom) pp 4–6

[29] Capuano L, Pohl R, Tiggelaar R M, Berenschot J W, Gardeniers J G E and Römer G R B E 2018 Morphology of single picosecond pulse subsurface laser-induced modifications of sapphire and subsequent selective etching *Opt. Express* **26** 29283

[30] Butkutė A, Baravykas T, Stančikas J, Tičkūnas T, Vargalis R, Paipulas D, Sirutkaitis V and Jonušauskas L 2021 Optimization of selective laser etching (SLE) for glass micromechanical structure fabrication *Opt. Express* **29** 23487

[31] Capuano L, de Zeeuw D and Römer G R B E 2018 Towards a numerical model of picosecond laser-material interaction in bulk sapphire *J. Laser Micro Nanoeng.* **13** 166–77

[32] Juodkazis S, Nishi Y and Misawa H 2008 Femtosecond laser-assisted formation of channels in sapphire using KOH solution *Phys. Status Solidi* **2** 275–7

[33] Jansen H V, Tas N R and Berenschot J W 2004 MEMS-based nanotechnology *Encyclopedia of Nanoscience and Nanotechnology* (Valencia, CA: American Scientific Publishers) pp 163–275

[34] Madou M J 2018 *Fundamentals of Microfabrication and Nanotechnology* (Boca Raton, FL: CRC Press)

[35] Bean K E 1978 Anisotropic etching of silicon *IEEE Trans. Electron Devices* **25** 1185–93

[36] Bassous E 1978 Fabrication of novel three-dimensional microstructures by the anisotropic etching of (100) and (110) silicon *IEEE Trans. Electron Devices* **25** 1178–85

[37] Seidel H, Csepregi L, Heuberger A and Baumgärtel H 1990 Anisotropic etching of crystalline silicon in alkaline solutions: II. influence of dopants *J. Electrochem. Soc.* **137** 3626–32

[38] Aota N, Aida H, Kimura Y, Kawamata Y and Uneda M 2014 Fabrication mechanism for patterned sapphire substrates by wet etching *ECS J. Solid State Sci. Technol.* **3** N69–74

[39] Liu C Y, Yeh C Y, Lai W H, Chou C Y, Li X F, Cheng C, Huang C K and Lai T L 2022 Wet-etching mechanism of a semi-sphere pattern on sapphire substrate *Mater. Chem. Phys.* **281** 125863

[40] Shen J, Zhang D, Wang Y and Gan Y 2017 AFM and SEM study on crystallographic and topographical evolution of wet-etched patterned sapphire substrates (PSS): I. Cone-shaped PSS etched in sulfuric acid and phosphoric acid mixture (3:1) at 230 °C *ECS J. Solid State Sci. Technol.* **6** R24–34

[41] Shen J, Zhang D, Wang Y and Gan Y 2017 AFM and SEM study on crystallographic and topographical evolution of wet-etched patterned sapphire substrates (PSS): part II. cone-shaped PSS etched in H_2SO_4 and H_3PO_4 mixture with varying volume ratio at 230 °C *ECS J. Solid State Sci. Technol.* **6** R122–30

[42] Xing Y, Guo Z, Gosálvez M A, Wu G and Qiu X 2020 Characterization of anisotropic wet etching of single-crystal sapphire *Sens. Actuators* A **303** 111667

[43] Lee Y J, Hwang J M, Hsu T C, Hsieh M H, Jou M J, Lee B J, Lu T C, Kuo H C and Wang S C 2006 Enhancing the output power of GaN-based LEDs grown on wet-etched patterned sapphire substrates *IEEE Photonics Technol. Lett.* **18** 1152–4

[44] Wu G, Xing Y, Chen Y and Zhou Z-F 2021 Application of the evolutionary kinetic Monte Carlo method for the simulation of anisotropic wet etching of sapphire *J. Micromech. Microeng.* **31** 065001

[45] Shang Y, Zhang H and Zhang Y 2021 Research on sapphire deep cavity corrosion and mask selection technology *Micromachines* **12** 1–10

[46] Zhang L *et al* 2020 Cavity etching evolution on the A-plane of sapphire crystal in molten KOH etchant *J. Cryst. Growth* **552** 125926

[47] Liu X Q, Zhang Y L, Li Q K, Zheng J X, Lu Y M, Juodkazis S, Chen Q D and Sun H B 2022 Biomimetic sapphire windows enabled by inside-out femtosecond laser deep-scribing *PhotoniX* **1** 99–102

[48] Oosterbroek R E, Berenschot J W, Jansen H V, Nijdam A J, Pandraud G, van den Berg A and Elwenspoek M C 2000 Etching methodologies in 111-oriented silicon wafers *J. Microelectromech. Syst.* **9** 390–8

[49] Matsuo S, Tabuchi Y, Okada T, Juodkazis S and Misawa H 2006 Femtosecond laser assisted etching of quartz: micro-structuring from inside *Appl. Phys.* A **84** 99–102

[50] Suratwala T *et al* 2020 Sapphire advanced mitigation process: wet etch to expose sub-surface damage and increase laser damage resistance and mechanical strength *Appl. Opt.* **59** 1602

[51] Zhang L, Sun J, Zuo H, Yuan Z, Zhou J, Xing D and Han J 2012 Tridimensional morphology and kinetics of etch pit on the {0001} plane of sapphire crystal *J. Solid State Chem.* **192** 60–67

[52] Zhou D, Li F, Yuan Z, Zhao Y, Zuo H, Han J, Zhang L and Sun J 2022 Cavity etching behavior on the M-plane of sapphire crystal *Cryst. Res. Technol.* 2200090

[53] Reisman A, Berkenblit M, Zirinsky S and Chan S A 1979 The etching of crystallographically determined orifices in sapphire *J. Electrochem. Soc.* **126** 1004–8

[54] Mustafa H, Matthews D T A and Römer G R B E 2019 Investigation of the ultrashort pulsed laser processing of zinc at 515 nm: morphology, crystallography and ablation threshold *Mater. Des.* **169** 107675

[55] Shah I A, van der Wolf B M A, van Enckevort W J P and Vlieg E 2008 Wet chemical etching of silicon {111}: autocatalysis in pit formation *J. Electrochem. Soc.* **155** J79–J84

[56] Shah I A, van der Wolf B M A, van Enckevort W J P and Vlieg E 2009 Wet chemical etching of silicon {111}: etch pit analysis by the Lichtfigur method *J. Cryst. Growth* **311** 1371–7